# Preparation of mesoporous $AgAlO_2$ by a two-step method with visible-light-driven photocatalytic activity

XIANGCHAO ZHANG*, ZHUO LUO, DIFA XU, SHIYING ZHANG*
*Hunan Key Laboratory of Applied Environmental Photocatalysis, Changsha University, Hongshan Road 98,Changsha, 410022, Hunan Province, P.R. China*

A novel visible-light-driven photocatalytic activity of mesoporous $AgAlO_2$ has been synthesized through a combined sol-gel and ion exchange method. The results demonstrate that the mesoporous $AgAlO_2$ is a delafossite structure with the uniform size about 20-40 nm and nitrogen adsorption-desorption type belongs to IV isotherms, the absorption edge of $AgAlO_2$ lies at 500 nm in the visible light region. The as-synthesized $AgAlO_2$ exhibited remarkably high photocatalytic activity of 82.38% in decomposing formaldehyde for 120 min under visible light irradiation. These results provide a basic experimental research for preparation Ag-based photocatalyst, which will possess a broad prospect in terms of the applications in improving indoor air quality.

(Received February 7, 2017; accepted February 12, 2018)

*Keywords:* $AgAlO_2$, Mesoporous, Visible-light-driven, Photocatalysis

## 1. Introduction

Nowadays, exploring the potential application of heterogeneous photocatalysis has attracted considerable interests in the fields of environmental remediation and energy conversion, such as water splitting, $CO_2$ reduction, thin film solar cell and contaminant degradation [1-3]. The metal oxide semiconductor nanostructures play an important role in the solar-to-chemical energy conversion due to their unique optical characteristics and catalytic properties [4]. However, broader applications of the typical $TiO_2$ are still limited due to its wide band gap and rapid recombination of photo-generated electron-hole pairs. Therefore, it is particularly important to design the advanced photocatalytic materials for the effective utilization of solar energy [5-6].

Recently, Ag-based photocatalyst as one of alternative visible-light-driven candidates have aroused much interesting due to the hybridization between Ag4d and O 2p orbital in the valence band, which can easily extend absorption spectrum into the visible light region meanwhile maintaining a strong oxidization potential [7-11]. On the other hand, increasing surface area is another efficient strategy in photocatalysis to improve activity. To gain mesoporous materials with ordered pore geometry, template strategies have been developed in the last two decades [12]. However, to the best of our knowledge, there are few reports on the mesoporous $AgAlO_2$ nanostructures.

Herein, we develop a novel visible-light-driven photocatalyst of mesoporous $AgAlO_2$ using a combined sol-gel and ion exchange method. The microstructure and optical properties of the as-prepared samples were investigated using XRD, SEM, TEM/HRTEM and UV-vis absorption spectra. The photocatalytic activity of as-synthesized sample is evaluated by the degradation of the formaldehyde under visible light irradiation. The proposed photocatalytic mechanism was also discussed.

## 2. Experimental

### 2.1. Preparation

All reagents were analytical grade and used without further purification or treatment. Mesoporous $AgAlO_2$ was synthesized by two-step method. Firstly, the precursor $NaAlO_2$ was prepared via a sol-gel method. In a typical procedure, 0.02mol $Al(NO_3)_3 \cdot 9H_2O$, 0.02mol $CH_3COONa \cdot 3H_2O$ and 1.0 g P123 surfactants were dissolved in 60 ml ethylene glycol ($C_2H_6O_2$), where P123 block-copolymer was used as a soft-template. The mixed solution was magnetically stirred for 5 h at 60-70°C to form yellow sol. The gel was further treated at 100°C for 12 h, after being sintered at 650°C for 4h to obtain mesoporous $NaAlO_2$ precursor. Secondly, $AgAlO_2$ was synthesized though the ionic exchange reaction. The powders of $NaAlO_2$, $AgNO_3$, and $KNO_3$ were mixed with molar ratios of 1:1:1 and grinded for 20 min [13]. Then the mixtures were heated to ion exchange at 250 °C for 12 h. The products were washed repeatedly with distilled water to remove $NaNO_3$, $KNO_3$, and excess $AgNO_3$. Finally, the mesoporous $AgAlO_2$ were obtained after the samples dried at 80 °C for 5-8 h. A schematic illustration is proposed by two step method in Fig. 1.

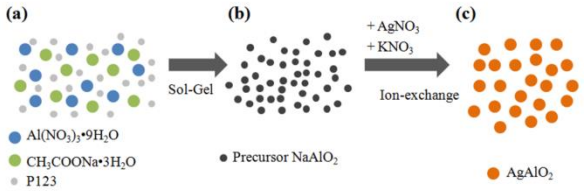


*Fig.1. Schematic illustration of the preparation of the mesoporous $AgAlO_2$*

### 2.2. Characterization

Structural features and phase compositions of the samples were determined using Bruker AXS D8 Advance X-ray diffractometer with Cu-Kα radiation (λ=0.15406nm). The surface morphology of as-prepared samples were observed using a field emission scanning electron microscope (FESEM JEOL Model JSM-6360LV) and high-resolution transmission electron microscopy (HRTEM, JEM-3010). The ultraviolet-visible (UV-vis) absorption spectra were acquired by UV-vis spectrometer (UV-2450, Shimadzu). The Brunauer-Emmett-teller (BET) specific surface area ($S_{BET}$) was determined by the AUTOSORB-IQ2-MP nitrogen adsorption apparatus (Quantachrome, USA).

### 2.3. Photocatalytic properties

The decomposition of formaldehyde was performed with visible light irradiation. In a typical process [14], 100ml formaldehyde solution (10 mg/l) was taken in the reactor along with 0.1g catalyst, and the mixture was irradiated under a 300 W Xe arc lamp through a UV cutoff filter (380 nm <λ < 750 nm). Before illumination the suspension was magnetically stirred in the dark for 30min to reach an adsorption/desorption balance of formaldehyde on the catalyst surface. The formaldehyde concentration was measured with a UV-vis spectrophotometer, the maximum absorption peak of formaldehyde was at λ= 414 nm. The degrading rate D was calculated as follow, $D=(C_0-C_t)/C_0\times100\%$, where $C_0$ is the initial concentration of formaldehyde (mg/l) and C is formaldehyde concentration at special time point (mg/l).

## 3. Results and discussion

The process involves in two basic steps, the precursor $NaInO_2$ was prepared by a sol-gel method and the mesoporous $AgAlO_2$ was prepared using ion exchange reaction. Fig.2 shows the microstructures of the as-prepared precursor $NaAlO_2$ and mesoporous $AgAlO_2$. For the precursor $NaAlO_2$, the typical XRD patterns reveals that all diffraction peaks can be well indexed to $NaAlO_2$ (JCPDS No. 33-1200). The precursor $NaInO_2$ show irregular morphologies with an average particle size of dozens to hundreds nanometer in addition to a certain degree of agglomeration in Fig. 1(b). The major diffraction peaks locate at 20.84°, 30.43°, 32.98°, 33.32°, 34.80°, and 39.56° are also observed in Fig.1(c), which correspond to the JCPDS No.21-1070 standard data of $AgAlO_2$ with delafossite phase. No diffraction peaks of the raw materials and other impurities were observed, indicating that the pure phase $AgAlO_2$ is formed and well crystallized through ion exchange reaction. The samples consist mainly of irregular particles with diameter about 50-200 nm in addition to a certain degree of agglomeration. The morphologies of the representative samples are also performed by using TEM/HRTEM. The TEM images in Fig. 3(a) show that the $AgAlO_2$ exist as irregular nanoparticles with size about 20-40 nm, and they tend to aggregate together. Benefiting from the low-temperature only 250 °C in the process of ion exchange reaction, it is difficult for $NaAlO_2$ to grow further or decompose, on the other hand, $KNO_3$ was used to promote the reaction, as a result, the morphologies and crystallite sizes from the precursor $NaAlO_2$ to mesoporous $AgAlO_2$ have no obvious change before and after ion exchange reaction. Therefore, it is assumed from the XRD results that the $AgAlO_2$ have been successfully prepared by the above two-step method.

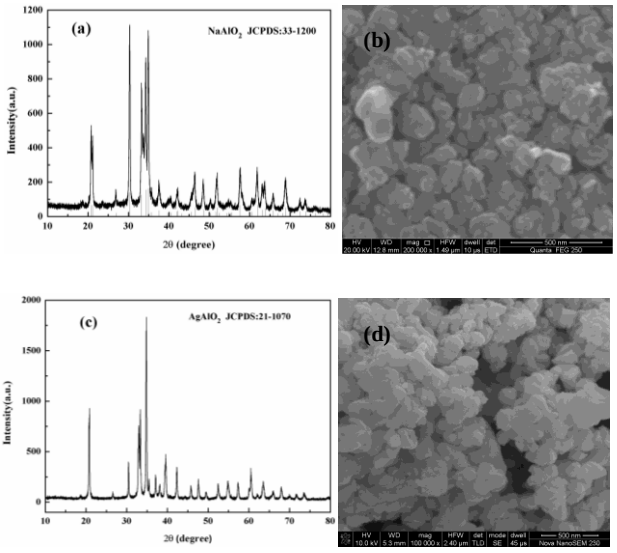


*Fig. 2. Microstructure of the as-synthesized samples (a) XRD patterns and (b) SEM image of the precursor $NaAlO_2$, (c) XRD patterns and (d) SEM image of the as-prepared mesoporous $AgAlO_2$, respectively*

Brunauer–Emmett–Teller (BET) gas sorptometry measurements were conducted to examine the porous nature of the samples. Fig. 3 reveals the nitrogen adsorption/desorption isotherms and pore size distribution curves of the prepared mesoporous $AgAlO_2$. According to IUPAC classification [15], the similar nitrogen adsorption-

desorption isotherms of samples can be classified as a type IV isotherm, and hysteresis loop is type $H_2$, which is characteristic of a typical mesoporous material. The sharp decline in the desorption curve and the hysteresis loop at high relative pressure are indicative of mesoporosity. During the process of adsorption, single molecular layer adsorption occurred at relatively low pressure and multi molecular layer adsorption occurred at higher pressure [16]. The calculated BET specific surface area and pore volume are 35.27 $m^2/g$ and 0.096 $cm^3/g$, respectively. From the inset figure, it can be seen that the average pore sizes of microstructure $AgAlO_2$ is about 9.12 nm. However, the shape of the curve exhibit a broad pore size distribution, suggesting that there is no ordering of mesopores, in contrast to the results known for mesoporous silica materials prepared with P-123. In the latter case, a much narrower pore size distribution can be achieved.

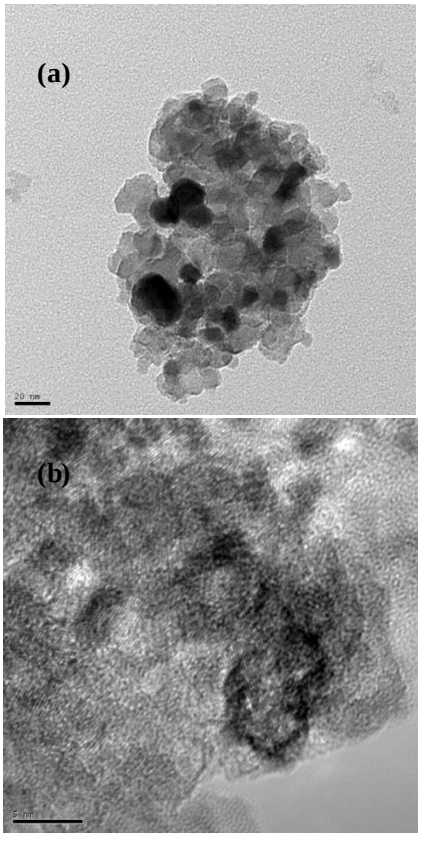


*Fig. 3. TEM/HRTEM images of the as-synthesized mesoporous $AgAlO_2$*

Fig. 4 displays the UV-vis absorption spectra of $AgAlO_2$, together with the P25 as a reference for a comparison. It can be observed that the absorption onset of the P25 is ~390 nm, which shows that the P25 is active mainly in UV light region, whereas $AgAlO_2$ shows obvious absorption in visible light region up to near 500 nm. The UV–vis absorption spectra show that absorption edge for mesoporous $AgAlO_2$ has a red shift compared with that of the P25, which shifts towards visible light region, which will probably make a good foundation for the investigation of mesoporous $AgAlO_2$ applied in the fields of improving indoor air quality.

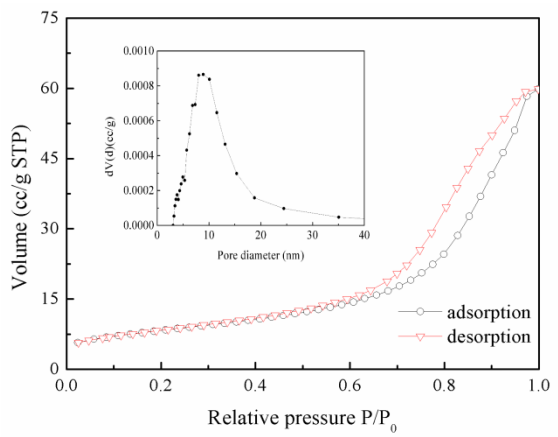


*Fig. 4. Nitrogen adsorption-desorption isotherms and pore size distribution curves (inset) of the as-prepared mesoporous $AgAlO_2$*

The photocatalytic activity of the commercial P25 and the as-prepared mesoporous $AgAlO_2$ were evaluated by the degradation of formaldehyde under visible light irradiations. The degradation rates of formaldehyde in the presence of different photocatalysts are discussed in Fig.5. Almost no change occurred in formaldehyde without catalyst under visible light, indicating direct photolysis of HCHO is negligible. When the commercial P25 sample is employed as photocatalysts, about 32.16% formaldehyde molecules are decomposed within 120 min under visible light irradiation. The result suggests that the obvious decrease of formaldehyde concentration in the presence of photocatalysts should be mainly contributed to the photocatalytic degradation. In the case of mesoporous $AgAlO_2$ under the similar experimental conditions, the degradation rate is 82.38% and the photocatalytic activity is enhanced by 50.22% comparing to that of the P25 photocatalyst. The reusability and stability of the Ag based photocatalysts are the other important factors in the practical applications. The repeated experiment of photocatalytic activities for degradation formaldehyde of the mesoporous $AgAlO_2$ under visible light irradiation in 5 recycles are shown in Fig. 6(b). There was a little appreciable loss in photocatalytic activity of the mesoporous $AgAlO_2$ after the five runs, the degradation rate is still 77.04%. This indicates that the photocatalytic activity of formaldehyde degradation is significantly enhanced for mesoporous $AgAlO_2$ than that for the Degussa P25 with visible light irradiation.

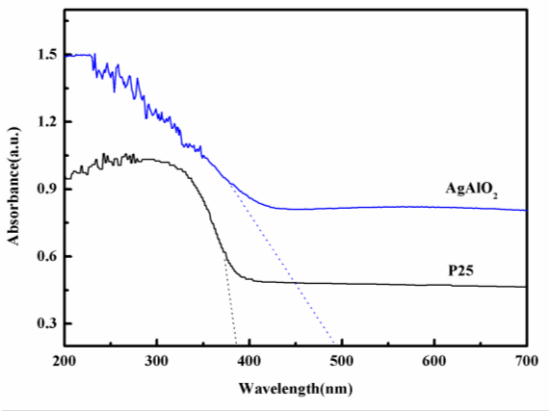


*Fig. 5. UV-vis absorption spectra of the commercial P25 and the mesoporous $AgAlO_2$*

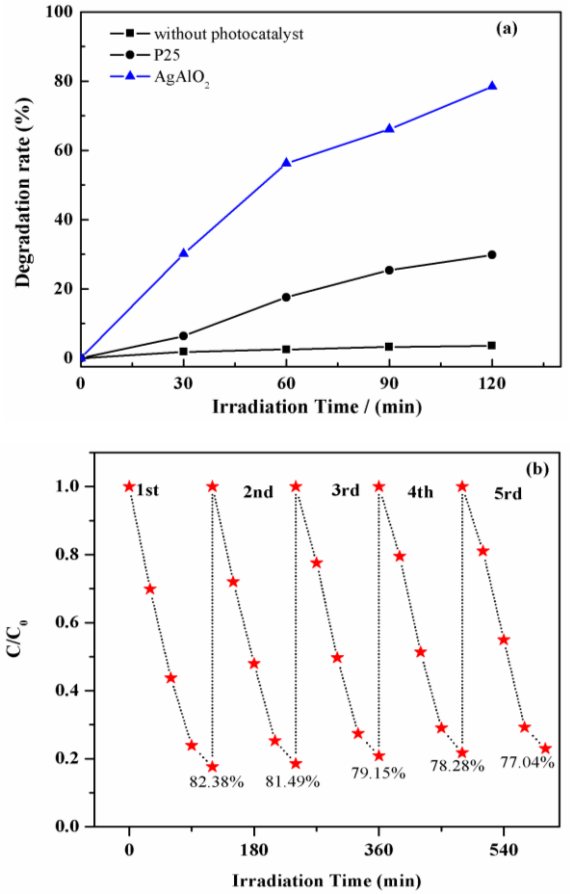


*Fig. 6. The photocatalytic properties of (a) degradation rates of formaldehyde in the presence of the P25 and mesoporous $AgAlO_2$ and (b) the reusability of the as-prepared mesoporous $AgAlO_2$ under visible light irradiation*

$AgAlO_2$ is a typical electron-conductive Ag-based semiconductor, the Ag 4d orbitals participate in the construction of VB which induces relatively localized photo holes, meanwhile, the CB of $AgAlO_2$ is about -0.638 eV which is more negative than the reduction potential of $O_2$( $H^+ + O_2 + e^- \rightarrow HO_2 - 0.046eV\ vsSHE$ ) [17]. Therefore, based on the above experimental results as well as reference [18-28], the proposed mechanism of the mesoporous $AgAlO_2$ for photocatalytic degradation formaldehyde under visible light irradiation can be described as follows:

$$AgAlO_2 + h\nu \rightarrow h_{VB}^+ + e_{CB}^- \quad (1)$$

$$O_2 + e_{CB}^- \rightarrow \cdot O_2^- \quad (2)$$

$$H_2O + h_{VB}^+ \rightarrow H^+ + \cdot OH \quad (3)$$

$$HCHO + \cdot OH \rightarrow \cdot CHO + H_2O \quad (4)$$

$$\cdot CHO + \cdot OH \rightarrow HCOOH \quad (5)$$

$$\cdot CHO + \cdot O_2^- \xrightarrow{+H^+} HCOOOH \xrightarrow{+HCHO} HCOOH \quad (6)$$

$$HCOOH \xrightarrow{\cdot O_2^- or \cdot OH} CO_2 + H_2O \quad (7)$$

## 4. Conclusions

In conclusion, the mesoporous $AgInO_2$ nanostructures have successfully been synthesized by a combined sol-gel and ion exchange method. The photocatalytic properties of the as-synthesized mesoporous $AgAlO_2$ degradation rates of formaldehyde reaches 82.38% for 120 min under visible light irradiation, which enhanced 50.22% than that of the commercial P25. Characterization results showed that the as-prepared $AgAlO_2$ with a delafossite structure has uniform size about dozens to hundreds nanometer and are indentified the isotherms as type IV. The absorption edge shows obvious absorption in the visible light range. There was a little appreciable loss in photocatalytic activity of the mesoporous $AgAlO_2$ after the five repeated experiment. This work provides some insight into the development of the mesoporous Ag-based nanostructures for improving indoor air quality by photocatalytic degradation formaldehyde under visible light irradiation.

**Acknowledgements**

This work was supported by the Program for the Hunan Provincial Natural Science Foundation of China (2016JJ6008), Scientific Research Fund of Hunan Provincial Education Department (17B029) and X. Zhang is grateful for financial support from the China Scholarship Council (201508430023).

## References


[1] J. Li, K. Zhao, Y. Yu, L. Zhang, Adv. Funct. Mater. **25**, 2189 (2015).
[2] X. Li, J. Yu, M. Jaroniec, Chem. Soc. Rev. **45**, 2603 (2016).
[3] Y. Wang, L. Du, L. Li, W. Zhang, Optoelectron. Adv. Mat. **10**(11-12), 950 (2016).
[4] X. He, J. Wang, Z. Shu, A. Tang, H. Yang, RSC Adv. **6**, 41765 (2016).
[5] F. Tian, H. Zhao, G. Li, Z. Dai, Y. Liu, R. Chen, Chem. Sus. Chem. **9**, 1579 (2016).
[6] X. Zong, L. Wang, J. Photochem. Photobio. C **18**, 32 (2014).
[7] S. Linic, P. Christopher, D. Ingram. Nat. Mater. **10**, 911 (2011).
[8] L. Wu, S. Fang, L. Ge, C. Han, P. Qiu, Y. Xin, J. Hazard. Mater. **300**, 93 (2015).
[9] J. Bi, Z. Zhou, M. Chen, S. Liang, Y. He, Z. Zhang, L. Wu, Appl. Sur. Sci. **349**, 292 (2015).
[10] H. Liu, D. Chen, Z. Wang, H. Jing, R. Zhang, Appl. Catal. B **203**, 300 (2017).
[11] X. Zhang, A. Tang, Y. Jia, Y. Wang, H. Wang, S. Zhang, J. Alloys Compounds **701**, 16 (2017).
[12] C. Bai, M. Liu, Angew. Chem. Int. Ed. **52**, 2678 (2013).
[13] S. Ouyang, Z. Li, Z. Ouyang, T. Yu, J. Ye, Z. Zou, J. Phys. Chem. C **112**, 3134 (2008).
[14] X. Zhang, Z. Luo, Y. Wang, S. Zhang, Chem. Lett. **45**, 1288 (2016).
[15] K. Sing, D. Everett, R. Haul, L. Moscou, R. Pierotti, J. Rouquerol, T. Siemieniewska, Pure Appl. Chem. **57**, 603 (1985).
[16] C. Li, Y. Jia, X. Zhang, S. Zhang, A. Tang, J. Cent. South Univ. **21**, 4066 (2014).
[17] S. Ouyang, J. Ye, J. Am. Chem. Soc. **133**, 7757 (2011).
[18] M. Khademalrasool, M. Farbod, A. Zad, J. Alloys Compounds **664**, 707 (2016).
[19] A. Tang, Y. Jia, S. Zhang, Q. Yu, X. Zhang, Catal. Commun. **50**, 1 (2014).
[20] L. Shi, D. Weng, Environ. Sci. **20**, 1263 (2008).
[21] D. Hu, Y. Xie, L. Liu, P. Zhou, J. Zhao, J. Xu, Y. Ling, Appl. Catal. B: Environ. **188**, 207 (2016).
[22] Y. Xie, D. Hu, L. Liu, P. Zhou, J. Xu, Y. Ling, J. Hazard. Mater. **318**, 551 (2016).
[23] P. Zhou, Z. Le, Y. Xie, J. Fang, J. Xu. J. Alloy. Compound. **692**, 170 (2017).
[24] F. Liu, Y. Xie, C. Yu, X. Liu, Y. Dai, L. Liu, Y. Ling. RSC Adv. **5**, 24056 (2015).
[25] P. Zhou, Y. Xie, J. Fang, Y. Ling, C. Yu, X. Liu, Y. Dai, Y. Qin, D. Zhou, Chemosphere **178**, 1 (2017).
[26] P. Zhou, Y. Xie, L. Liu, J. Song, T. Chen, Y. Ling, RSC Adv. **7**, 16484 (2017).
[27] C. Sun, Q. Xu, Y. Xie, Y. Ling, J. Jiao, H. Zhu, J. Zhao, X. Liu, B. Hu, D. Zhou, J. Alloys Compounds **723**, 333 (2017).
[28] X. Zhang, D. Xu, Y. Jia, S. Zhang, RSC Adv. **7**, 30392 (2017).



*Corresponding author: cdzhangshiying@163.com
csuzxc@126.com